

# Towards High-Power Microwaves

S.Anishchenko, V.Baryshevsky, A.Gurinovich,  
E.Gurnevich, P.Molchanov, A.Rouba.

*Institute for Nuclear Problems of Belarusian State University &  
Electrophysical laboratory, Minsk, Belarus*

November 11, 2022

## Abstract

In this paper, we review and compare HPM sources operating without a magnetic field to guide the electron beam that are capable of producing high-power microwave (HPM) pulses with a duration of about 100 ns. The proposed analysis summarizes multi-year research carried with three types of HPM sources: a split-cavity oscillator (SCO); an axial vircator; and a virtual cathode oscillator in Reflex Triode geometry. These options were simulated for electron beam energy  $\sim 400$  keV and for pulsers with demonstrated capability to provide high power microwave pulses with the required pulse duration. Designed sources were experimentally tested, and their advantages and weaknesses are discussed with respect to high output power, long pulse duration, and good operating stability.

## 1 Introduction

The aim of the presented analysis is to compare HPM sources of different types and substantiate the choice of a source that will provide high output power, long pulse duration and good operating stability. The technical requirements for the HPM source are operation without a magnetic field and compact design. Single frequency operation during the 100 ns pulse is desired.

Three types of HPM sources which comply with the above features are analyzed and compared, namely: a split-cavity oscillator (SCO), an axial vircator and a virtual cathode oscillator in Reflex Triode geometry (referred hereinafter as reflex triode).

Split-cavity oscillator (SCO), as proposed in [1], is a compact device, whose self-excited oscillating electromagnetic field converts a steady electron beam into one with highly modulated density. Short travel length eases overcoming both space-charge and pinching limitations, thus, enabling high currents and quite high input power.

Devices based on the virtual cathode principle operate at a current density that exceeds the space charge limit [2–6]. High input power somewhat compensates low intrinsic efficiency, which nevertheless could be increased by inserting resonant elements into the beam-wave interaction area. An HPM source with a virtual cathode is usually composed of a few elements: vacuum diode with a cathode emitting electrons and mesh anode letting the electron beam to enter the resonant cavity, which design could be elaborate though.

Differences in operation mechanism, electron beam dynamics, source impedance and radiation mode for all three types of sources make comparison challenging. We have

chosen the following parameters for comparison: output radiation power, duration of radiated pulse, operation stability (reproducibility of results).

Each of three sources we tested was designed to operate at electron beam energy  $\sim 300\text{--}500$  keV. The typical current values for SCO ranged from 3 to 8 kA, for virtual cathode oscillators they were expectedly higher: 13-20 kA.

Barrel-type housing rendered volume available for evacuation and placing the structure (resonator), inside which the electron beam interacts with electromagnetic field. HV was applied to the core conductor from the high-voltage pulse source; vacuum feed-through isolator bounded the evacuated volume from one face, another face was covered by the output window. HV pulse polarity, either negative for axial vircator and SCO or positive for reflex triode, was determined by the power supply. The applied voltage and the beam current were measured to evaluate the input power. Source impedance was varied by changing the cathode-anode gap and the diameter of cathode. Cathodes of different types were tested, resonant elements in composition of each source were used for fine tuning radiation output.

Radiated electric field strength was measured in the direction of its maximal value at some distance from the output window and reduced to 1 meter distance. Output power was evaluated considering HPM source directivity and was used for efficiency calculation. Output power values in this paper are averaged over several oscillation periods. Radiated time-domain waveform was analyzed to reveal its spectral content and power distribution within the pulse duration interval.

This paper is focused on summarizing and comparing the results obtained experimentally. Each subsequent section 2 - 4 presents the experimentally obtained results and discusses the observed advantages and weaknesses of each source. Conclusive section discusses comparison results.

## 2 SCO

The split-cavity oscillator proposed in [1] was operating at 100-150 kV to radiate at  $\sim 1$  GHz. A high-quality pillbox cavity with conducting screen walls, through which an electron beam could pass, was partitioned (split) by a screen leaving a gap between it and the outer cavity wall. The self-excited electromagnetic field oscillating at the frequency of fundamental mode of the split cavity enabled converting a steady electron beam into highly density modulated one. Conducting screen walls and split meshes also served for beam guiding: radial electric field component was reduced, thus, reducing Coulomb repulsion in the beam without the need for an applied magnetic field. The extractor collected the exit beam on an inverse diode in a wave matching area and launched an electromagnetic wave into a coaxial transmission line and output horn.

A disadvantage of the above SCO was the strong compression of electron beam [7] exiting the pillbox by its own magnetic field that caused plasma emission from the extractor face due to electron bombardment and, thus, radiation failure.

Experimental studies [8, 9] demonstrated possibility of SCO operation at higher frequencies at 400 – 500 kV producing power 200–400 MW. Operation of SCO at high beam energies was considered in [10]. SCO cavity split to unequal parts was studied in [9, 11, 12].

We designed and tested two split-cavity oscillators to operate at 300–400 kV and  $\sim 3$  GHz using the approaches [1, 7–10]. Similar [1] the split mesh was used in SCO design option #1 (see Fig.1,2), while in the design option #2 we replaced mesh with a split diaphragm (see Fig.3).

In SCO design option #1 pillbox was used for electron beam modulation and wave matching area between SCO and extractor served for beam energy conversion to radiation.

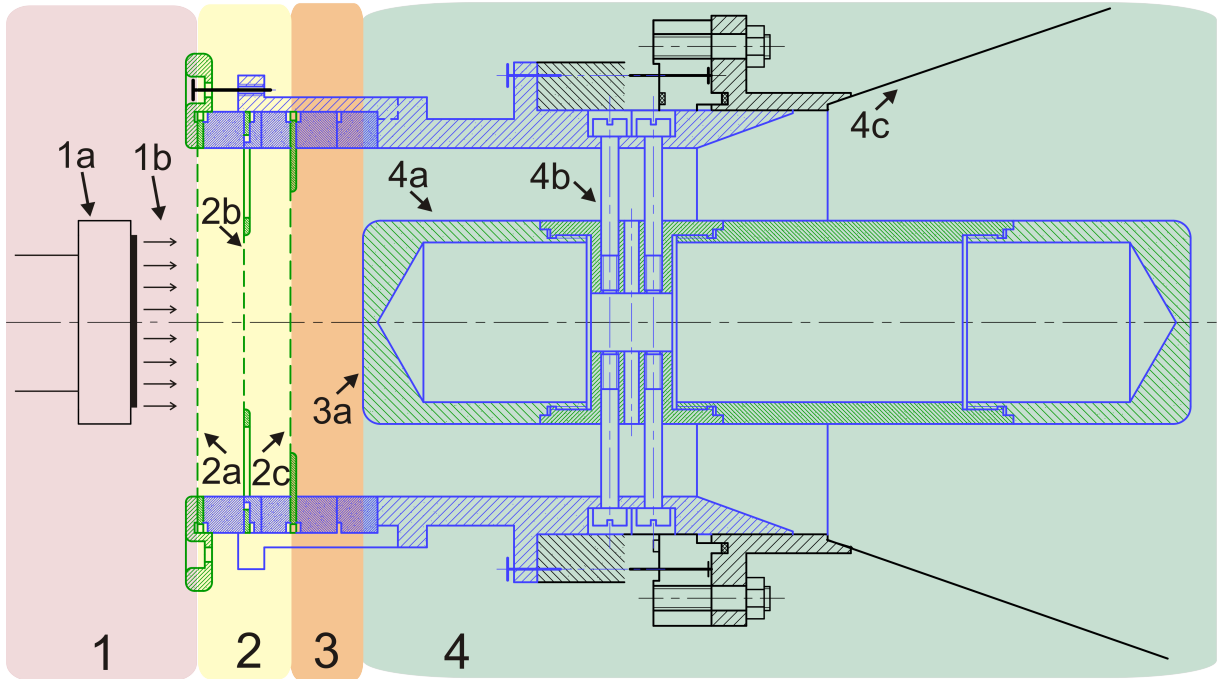


Figure 1: SCO design option #1:

1 – vacuum diode; 1a – graphite cathode  $\varnothing$  50 mm, 1b – cathode-anode gap 14 mm;  
 2 – pillbox #1 with length 28 mm and inner  $\varnothing$  120 mm: 2a – anode mesh (mesh #1), 2b – split mesh with  $\varnothing$ 90 mm, 2c – mesh #2 with  $\varnothing$ 90 mm with support ring;  
 3 – pillbox #2 with length 20 mm and inner  $\varnothing$  120 mm: 3a – extractor face serving to absorb e-beam;  
 4 – wave matching area: 4a – extractor with length 285 mm,  $\varnothing$ 70 mm, 4b – extractor supports, 4c – horn with length 550 mm,  $\varnothing$ 480 mm

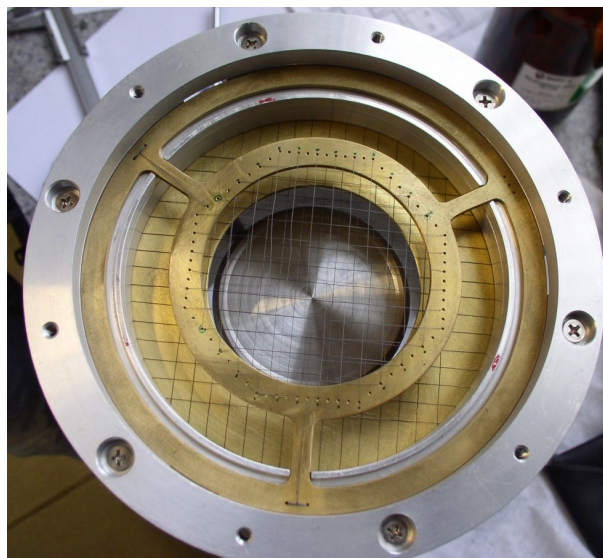


Figure 2: Disassembled SCO design option #1, split mesh and metal extractor can be seen (see Fig. 1)

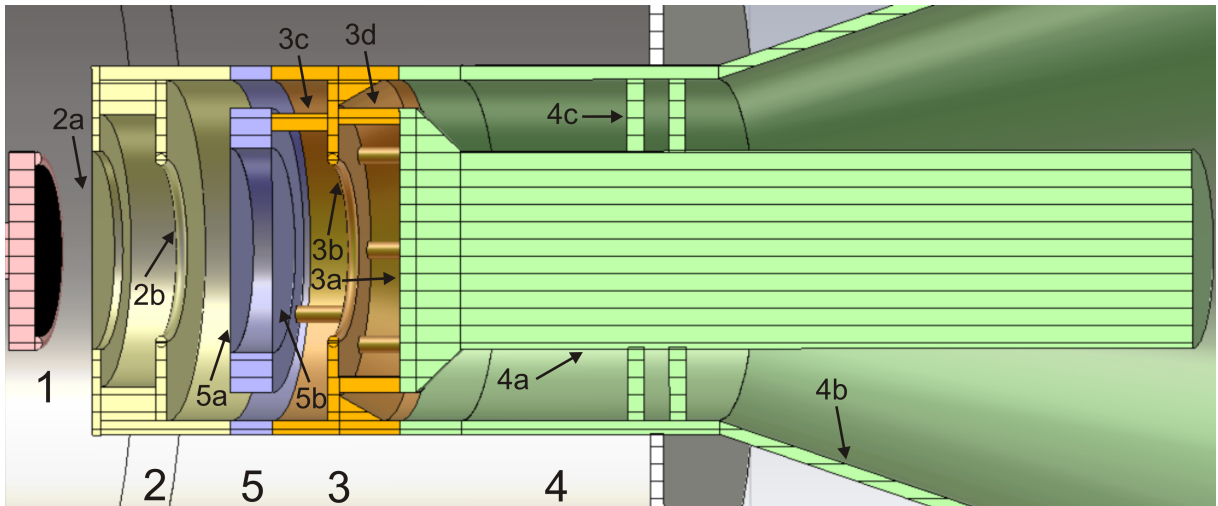


Figure 3: SCO design option #2 (with split diaphragms):

- 1 – vacuum diode with carbon-multicapillary cathode  $\varnothing$  60 mm and cathode-anode gap 16-20 mm;
- 2 – pillbox #1 with length 50 mm and inner  $\varnothing$  120 mm: 2a – anode mesh (mesh #1), 2b – split diaphragm #1 with inner  $\varnothing$ 60 mm;
- 3 – pillbox #2 with length 44 mm and inner  $\varnothing$  120 mm: 3a – extractor face serving to absorb e-beam, 3b – split diaphragm #2 with inner  $\varnothing$ 60 mm, 3c – drift chamber supports, 3d – metal extractor supports;
- 4 – wave matching area: 4a – extractor with length 285 mm, input/output  $\varnothing$ 100/70 mm, 4b – horn with length 550 mm,  $\varnothing$ 480 mm, 4c – dielectric extractor supports;
- 5 – drift chamber with length 15 mm, outer/inner  $\varnothing$ 100/72 mm: 5a – mesh #2, 5b – mesh #3

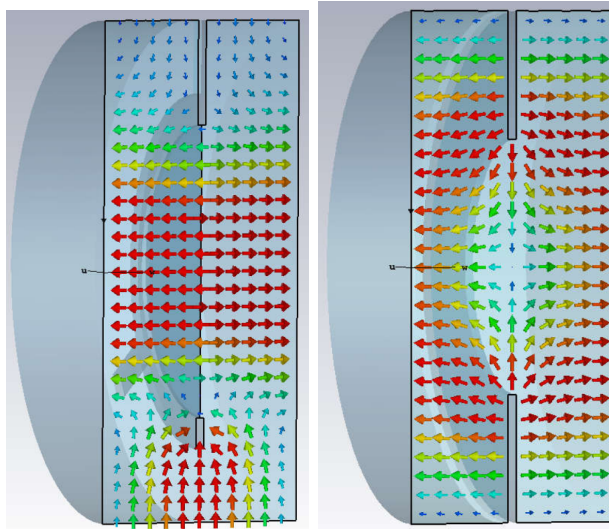


Figure 4: RF electrical field of the fundamental mode in SCO cavity design option #1 (left) and design option #2 (right)

SCO design option #2 was composed of two pillboxes with a drift chamber between them: the first pillbox in this case modulated the beam, the second one served for beam energy conversion to radiation. In contrast to [8, 9] we used split diaphragms instead of split meshes. Such replacement enabled to reduce multiple scattering of beam electrons by the meshes and to eliminate all the associated effects. Additionally, electron beam compression was reduced.

Coupling of two pillboxes was enabled by design of drift chamber placed with a gap between it and the outer cavity wall that enabled field oscillation in a joint volume without special SCO cavities tuning.

For SCO design option #1 we tested two variants of extractors: that purely metal and covered with graphite. Applying graphite cover to an extractor is beneficial for output power because of lower albedo for graphite as compared to metal [13]. Therefore for SCO design option #2 we used only extractor covered with graphite.

Similar [8, 9] duration of radiation pulse (approximately 10 ns) in our experiments was much shorter than current pulse width, which was about 100 ns. We explained this by plasma formation inside the cavity and wave matching area; use of duralumin for manufacturing the SCO parts exacerbated the situation because of oxide film on all the surfaces. Multiple scattering and secondary electron emission from all the parts bombarded by the electrons also contributed.

Input and output parameters for both SCO design options are gathered in Table 1.

RF electrical field of the fundamental mode in SCO cavity determines SCO operation frequency (comparison of field structure for SCO with the split mesh and that for the cavity with the split diaphragm is given in Fig. 4). That is why change of the gap between the anode and the cathode does not influence the radiation frequency (see Fig. 6). Gap change can influence radiation only via impedance and beam current change.

Experiments with SCO demonstrated stable single-frequency operation. Detected output power was as high as 30 MW and efficiency was  $\sim 2\%$ . However, the duration of radiation pulses were much shorter than the width of the current pulse (see Table 1) despite the fact that start of HPM generation occurred at growing voltage and current in vacuum diode (well before the maxima of voltage and current).

Pulse shortening was explained by enhancement of electric field within small gaps inside the SCO structure and plasma therein. Power growth could also be limited by breakdown, similar reasons limiting MILO operation in [14, 15].

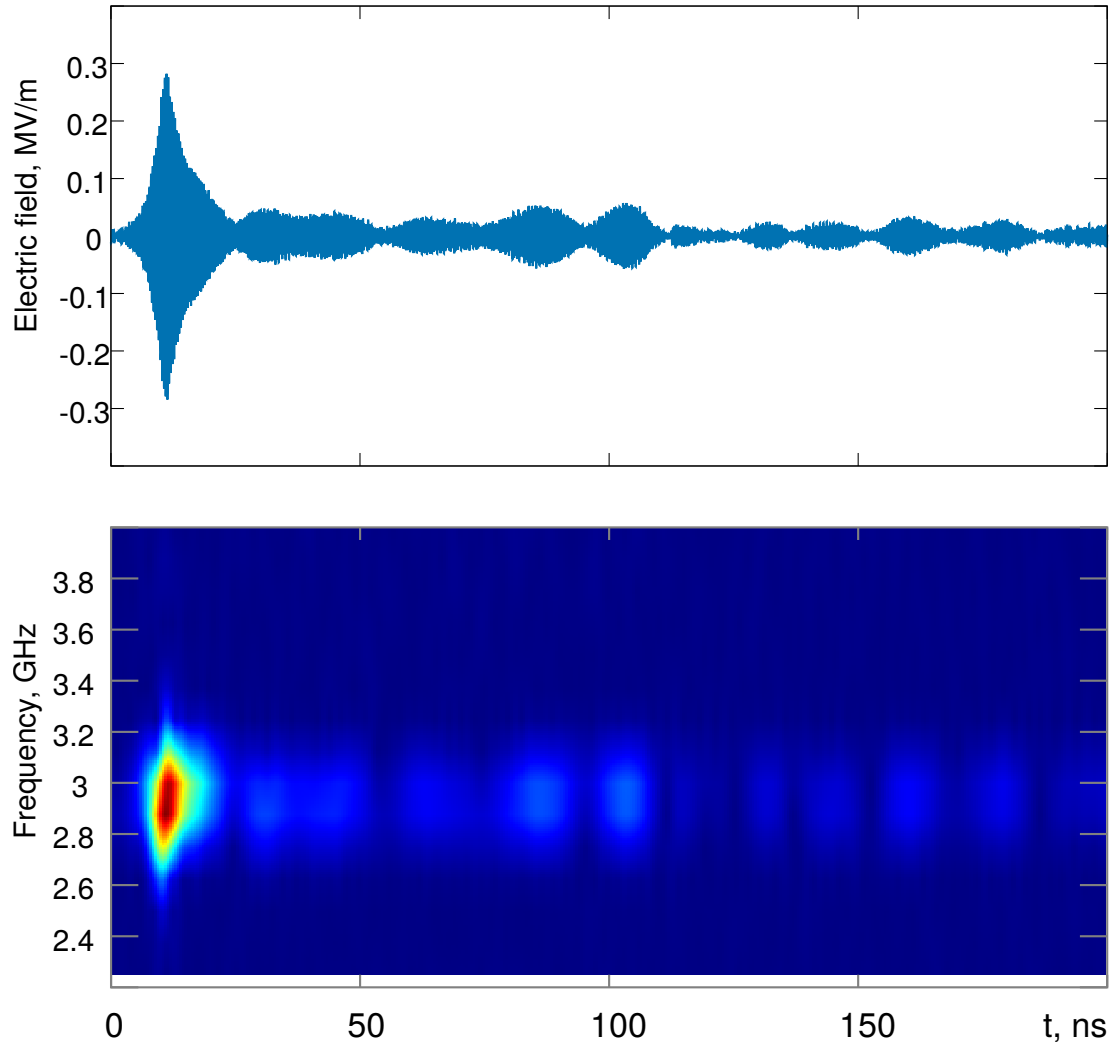


Figure 5: Detected microwave signal with the highest amplitude and its spectrogram for SCO design option #2

All the measures reducing multiple scattering, secondary electron emission and electric field strength inside SCO structure would be beneficial for both output power and pulse duration. SCO designed for operation at lower frequency has some advantages, since the dimensions of SCO structure and all the gaps are expected to be larger.

Simulated and experimental results showed that the stability of the observed results was high, but the experimental results showed that the radiated power and pulse duration were low when compared to the simulation. Analysis of the results enabled us to assume that pulse shortening was being caused by secondary electron emission inside the SCO and by the expanding plasma cloud, which is formed in the vicinity of the extractor as a result of its being bombarded by electrons causing the beam to be compressed by its own magnetic field.

Table 1: Input and output parameters of HPM sources on the base of SCO.

No.	Parameter	SCO design option #1	SCO design option #2
1	Voltage at start of HPM generation	300 kV	350 kV
2	Current at start of HPM generation	8 kA	4 kA
3	HPM frequency	$\sim 3$ GHz	
4	E-field @ 1 meter	300 kV/m @1m	250 kV/m @1m
5	Radiated pulse FWHM	$\sim 10$ ns	$\sim 5$ ns
6	Power density	125 MW/m <sup>2</sup>	85 MW/m <sup>2</sup>
7	Power	$\sim 30$ MW	
8	Efficiency	1.3 %	2.1 %

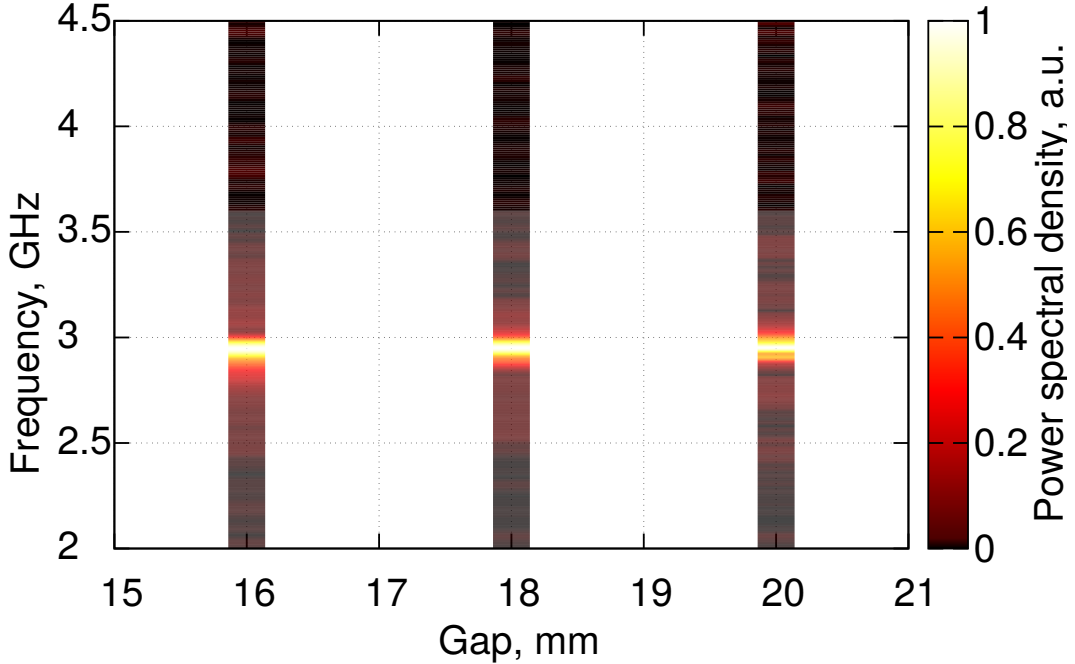


Figure 6: Comparison of spectra for SCO with split diaphragms obtained for different cathode-anode gap values

### 3 Axial vircator

Different vircator designs with resonant cavities were proposed [16–19]. The studies of axial vircators with multicavity resonators proved the possibility of a resonant increase in the efficiency [20–22].

Using [22] as a starting point for the development, we designed several resonators for the three-cavity axial vircator [23, 24] (see one of them in Fig. 7). In simulation [24, 25] the axial vircator designed for operation in the frequency range from 3 to 4 GHz at 450 keV demonstrated efficiency greater than 5% and the power reached 350 MW at 3.2 GHz (mind that both simulated and observed values shown in [24] and [23], respectively, refer to the instantaneous (peak) power rather than the average power we are using in the present article).

Experiments with the designed axial vircator [23] were focused on investigation of output power and operation stability for cathodes of different type and size, varied cathode-anode gap.

Solid and ring-type cathodes made of dense fine grained graphite, and multi-capillary

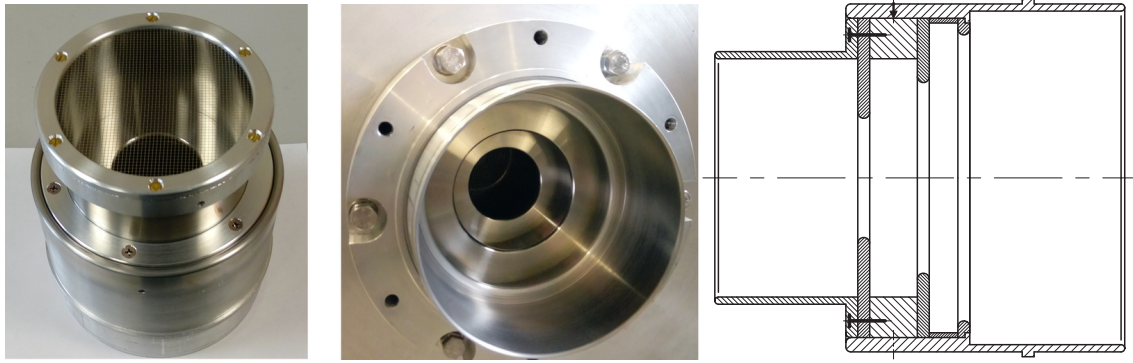


Figure 7: Three cavity resonator of axial vircator [23]: outside view with mounted anode mesh (left), inside view (mesh is unmounted, middle), drawing (left)

cathodes, which emitter was formed by an array of carbon-epoxy capillaries were used (see Fig. 8). Outer diameter of graphite cathodes varied from 60 to 71 mm; inner diameter for ring-type graphite cathodes used in the experiments ranged from 20 to 26 mm. Engraved concentric grooves on flat emitting surface of each cathode facilitated uniform emission. Two types of multicapillary cathodes with outer diameter of emitting area varying from  $\sim 60$  mm to  $\sim 70$  mm were tested: the first one was similar to solid graphite cathodes (see Fig. 8, bottom left), and the second one was similar to ring-type graphite cathodes (inner diameter of emitting area was varied from  $\sim 21$  mm to  $\sim 28$  mm, see Fig. 8, bottom right).

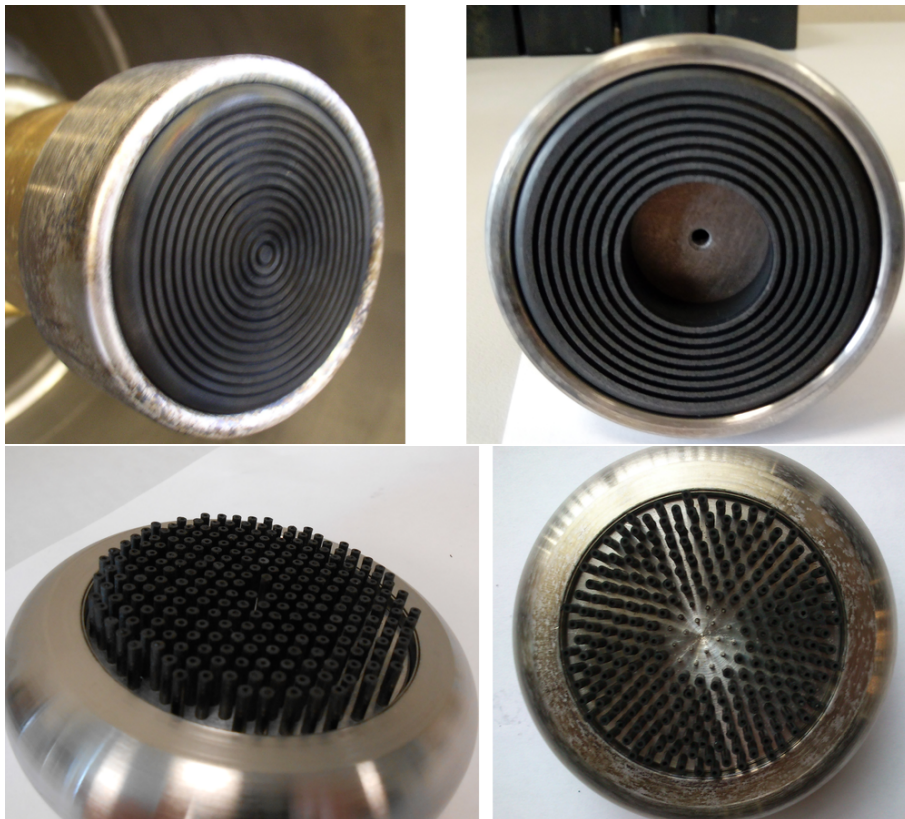


Figure 8: Solid (top left) and ring-type (top right) cathodes made of dense fine grained graphite; solid (bottom left) and ring type (bottom right) multi-capillary cathodes

In all experiments with the solid graphite cathodes the observed power was lower than predicted in simulation [24]:  $\sim 30$  MW for  $\varnothing 60$  mm cathode and  $\sim 60$  MW for cathode with  $\varnothing 71$  mm.



Ring-type graphite cathode with outer diameter 60 mm enabled us to achieve the power values close to those predicted in [24] (up to 300 MW). The progressive enlargement of the cathode inner diameter from 20 mm to 24 mm, when keeping all other parameters the same, resulted in an increase of the radiation power to 150 MW and even to 300 MW in several shots (see Fig. 9). Increase of inner diameter from 24 to 26 mm led to decrease of microwave signal. Duration of radiation pulse for shots with high output power attained 50 ns. Direct correlation of radiation pulse duration with that for current pulse was not observed: FWHM for current pulse was as high as 150–200 ns. We explained this fact by high-voltage breakdown and plasma formation inside the resonator.

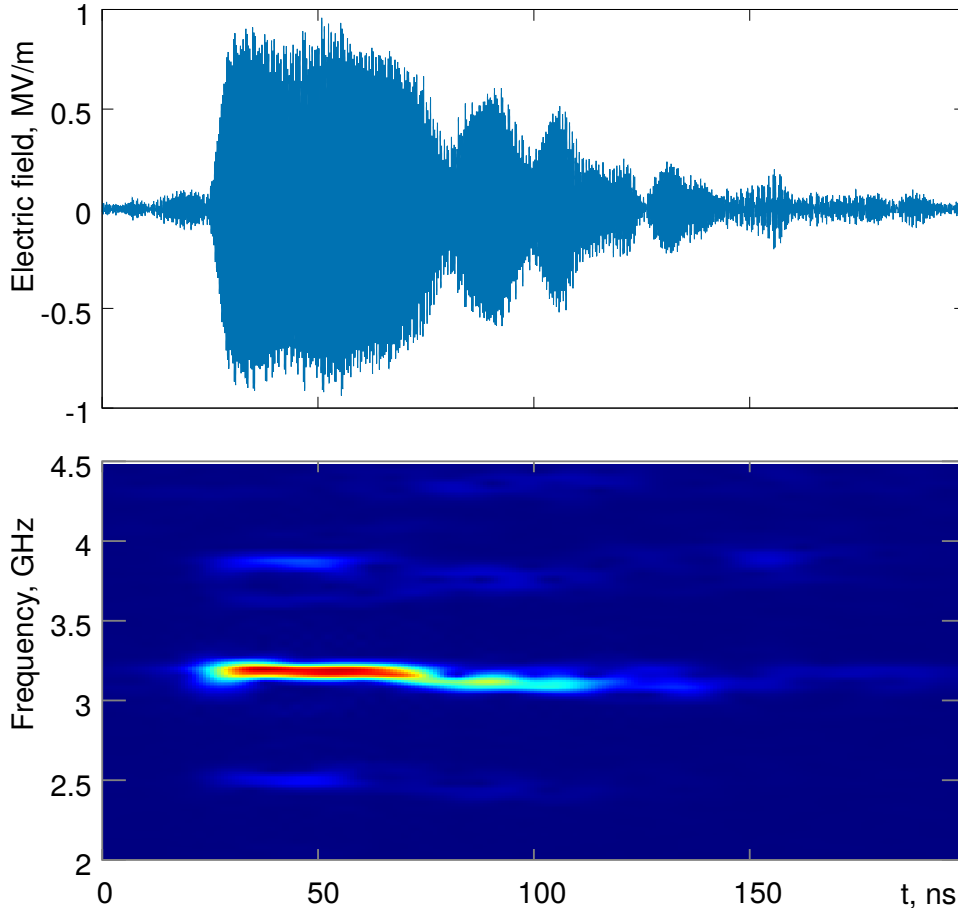


Figure 9: Detected microwave signal with the highest amplitude and its spectrogram for the axial vircator with multicavity resonator, graphite ring-type cathode with outer/inner diameters 60/24 mm and cathode-anode gap 16 mm [23]

Comparison of simulation results [24] and data obtained experimentally [23] demonstrated perfect fit in basic frequency and accordance in radiated power. However, the experiments demonstrated low reproducibility of results though the operation parameters in the utmost and ordinary cases seemed to be identical. The subsequent analysis [25] explained the unstable operation by high dependence of axial vircator efficiency on the spread of the electron velocities in the beam: growth of the momentum (energy) spread from 1% to 5% caused drop of the efficiency from 6% to  $\sim 1\%$ .

Multi-capillary cathodes were put for tests in anticipation of higher output due to more uniform electron beam with lower energy spread as compared to graphite cathodes. However, radiation output produced by all variants of multi-capillary cathodes was the same as recorded in the shots with the solid cathodes made of dense fine grained graphite.

Experiments with the ring-type cathodes revealed one more challenge: we observed extremely fast damage of the anode mesh. Additional studies showed that this phenomenon was due to electrostatic cumulation of high-current electron beam [26, 27].

According to simulation the cathode-anode gap mainly influences on the radiation spectra [28, 29]: when the cathode-anode gap was reduced to appear below a certain value, the basic vircator frequency grew. This is due to increase of electron-beam plasma frequency [5, 6]. We also observed such frequency behavior in the experiments [23] (see Fig. 10). With the cathode-anode gap varying from 14 mm to 17 mm, the microwave pulse duration, and the peak power remained almost the same; but further increase of gap led to power reduction and the microwave pulse delay with respect to the current pulse. At the same time for each cathode-anode gap value the radiation frequency weakly depended on beam current.

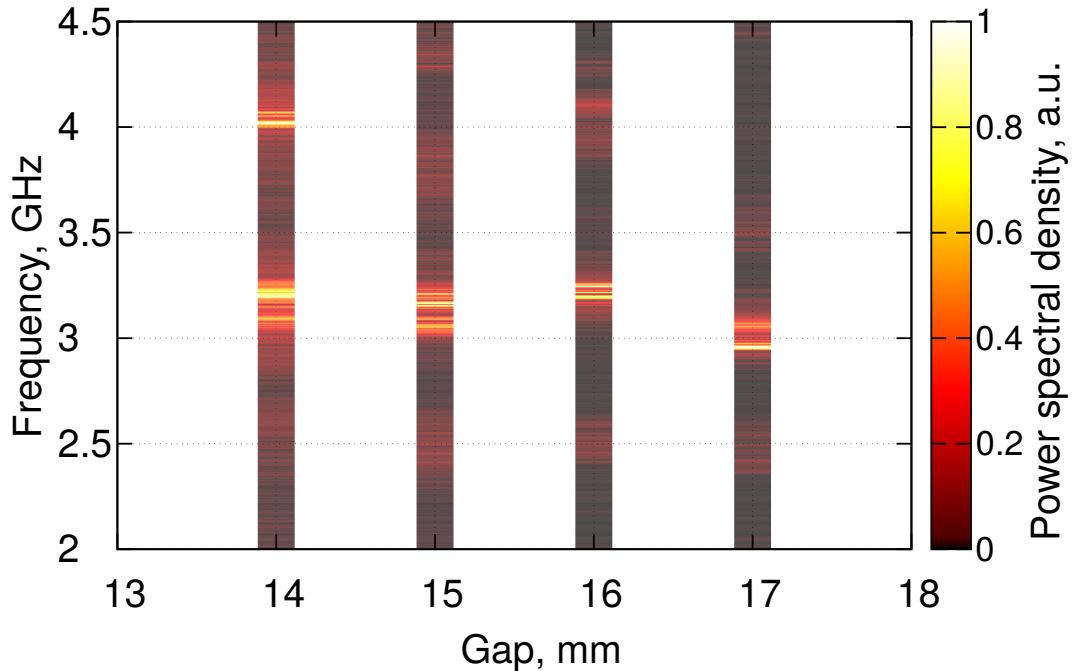


Figure 10: Comparison of axial vircator spectra obtained for different cathode-anode gap values [23] for solid graphite cathode of 60 mm diameter

Stability of axial vircator operation in our experiments was low and in many cases the radiated power was much lower than simulation had predicted. The subsequent analysis [25] explained the unstable operation by high dependence of source efficiency on the spread of electron velocities in the beam. Nevertheless, by testing different cathode shapes, materials and operation conditions we succeeded to achieve efficiency about 5% and power up to 300 MW at 3.2 GHz. Ring-type graphite cathode with outer/inner diameters 60/24 mm produced radiation power from 150 MW to even 300 MW in several shots. Duration of radiation pulse was about 50 ns at FWHM for current pulse as high as 150–200 ns. We explained this fact by high-voltage breakdown and plasma expansion inside the resonator and cathode-anode gap. Extremely fast damage of the anode mesh was explained by electrostatic cumulation of high-current electron beam.

## 4 Reflex triode

A virtual cathode oscillator operating in reflex triode geometry [5, 16, 30–34] has all the strengths and weaknesses typical for this type of HPM sources, particularly it demon-

strates relatively low efficiency. However, introducing a resonant feedback into the system, one could enhance the efficiency (up to 10%-12%) and single-frequency operation [4, 22, 30, 35–38]. A vircator placed into a resonator, whose natural frequency is close to the virtual cathode oscillator frequency, attains the above resonant feedback. In [30] the performance of a reflex triode was modified with the inclusion of reflecting strips that provided increase of microwave peak power output to 330 MW at 11% efficiency.

Following the concept of vircator with resonant feedback we developed the reflex triode with shiftable reflectors (see Fig. 11) and experimentally studied its performance [38]. Radiation frequency, output power and duration of radiation pulse were analyzed for different cathode-anode gap values, cathode materials and varied reflector positions. System parameters ensuring high operating stability at single frequency ranging from 3.0 to 4.2 GHz and high-power operation with long pulse duration were obtained.

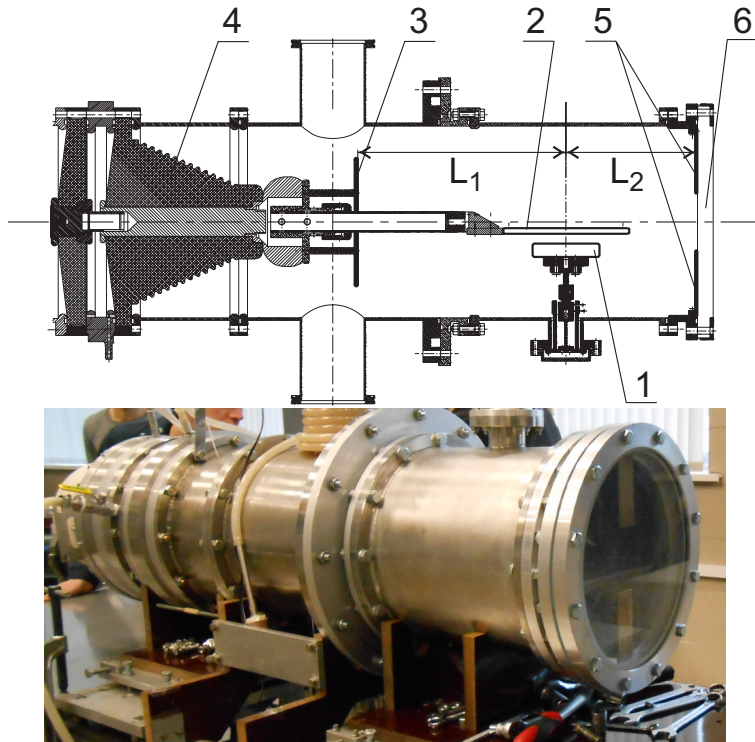


Figure 11: Reflex-triode geometry (top) and photo (bottom): 1 – the explosive-emission cathode, 2 – anode mesh and anode holder centered in the vacuum chamber, 3 – disk-shaped reflector, 4 – high-voltage vacuum feed-through, 5 – shiftable reflector with rectangular brass stripes, 6 – output window

The reflex-triode geometry can be described as follows. The vacuum chamber of 300 mm diameter encloses the triode reflex geometry vircator (see Fig. 11):  $L_1$  and  $L_2$  are the variable distances from the cathode axis to the disk-shaped and output shiftable/removable reflectors, respectively. Stainless steel woven anode mesh with 77% geometric transparency was used in the experiments; the diameter of the mesh thread is  $224 \mu\text{m}$ . Solid type cathodes were made of different materials: fine-grained graphite MPG-8, duralumin, steel nails, carbon-epoxy capillaries. The output reflector consisted of two rectangular brass stripes 40 mm in width and 100 mm in length, housed at a variable distance from the cathode axis, normally to the anode plane position.

The value of the cathode-anode gap was assured with 0.1 mm accuracy. Coplanarity of cathode and anode surfaces was controlled. The cathode-anode gap value and positions of both reflectors (defined by  $L_1$  and  $L_2$ ) were tuned in order to observe stable single frequency generation and the highest output power. A pulsed power supply, similar to

that in [23], was used to drive the HPM source.

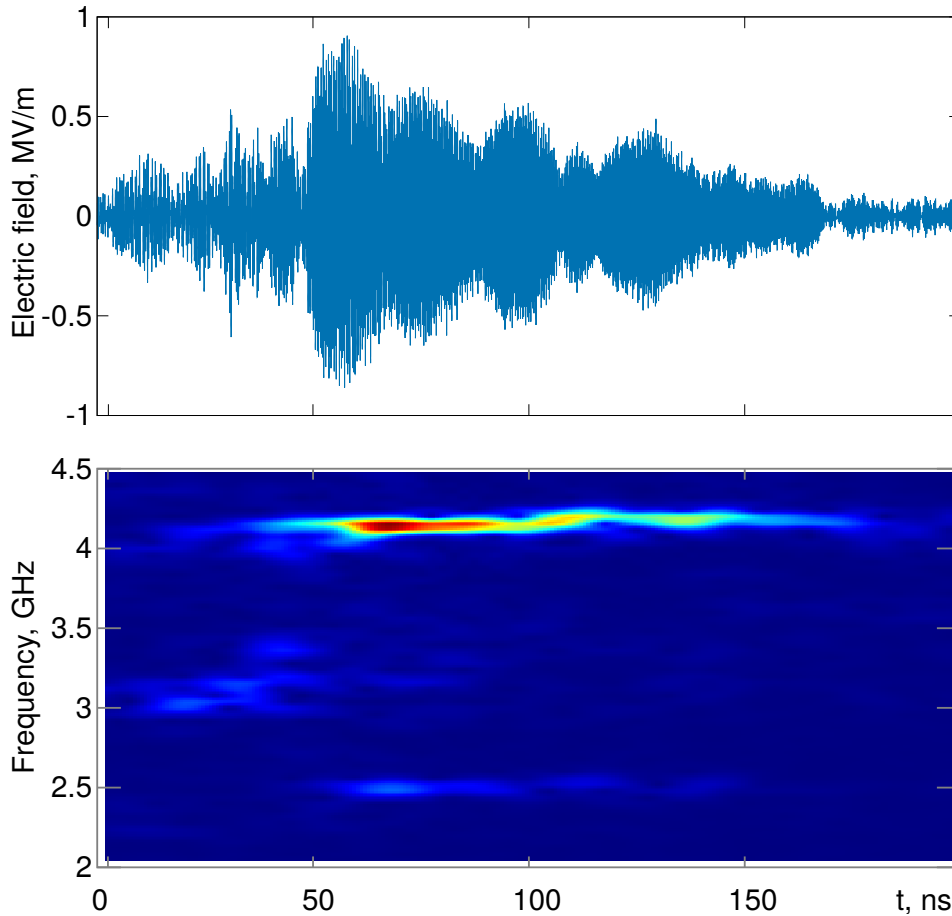


Figure 12: Detected microwave signal with the highest amplitude and its spectrogram

The maximum radiated power was observed at cathode-anode gap 16 mm and reflector positions  $L_1 = 290$  mm and  $L_2 = 164$  mm. As much as 460 MW was produced at 4.16 GHz single-frequency operation at maximum diode voltage 460 kV and amplitude of electron beam current 18 kA. Detected microwave signal with electric field strength amplitude  $\sim 800$  kV/m @ 1 m and its spectrogram are shown in Fig. 12. The cathode-anode gap increase to 17 and 18 mm resulted in spectrum broadening and shift of its central frequency.

The most stable operation of the reflex triode was observed when output reflector was removed. The corresponding spectrogram is shown in Fig. 13. The main feature of the configuration is the usage of multicapillary cathodes (see Fig. 14) described in [39]. It is found that this type of cathodes provides the most stable single-frequency operation at 200 MW.

Duration of radiation pulse correlated with FWHM of current pulse: when duration of current pulse was increased from 150 to 250 ns, the microwave pulse duration grew from 50 to 150 ns. This was in contrast to operation of axial vircator, where high-voltage breakdowns and plasma expansion inside the resonator and cathode-anode gap limited duration of radiation pulse.

It should be noted that in order to avoid the impact of powerful microwave radiation on the vacuum pumps, they are turned off before every shot. At this time, evacuation is carried out by getter pumps. Moreover, the presence of vacuum pumps make us try-out sealing of the reflex triode in its design.

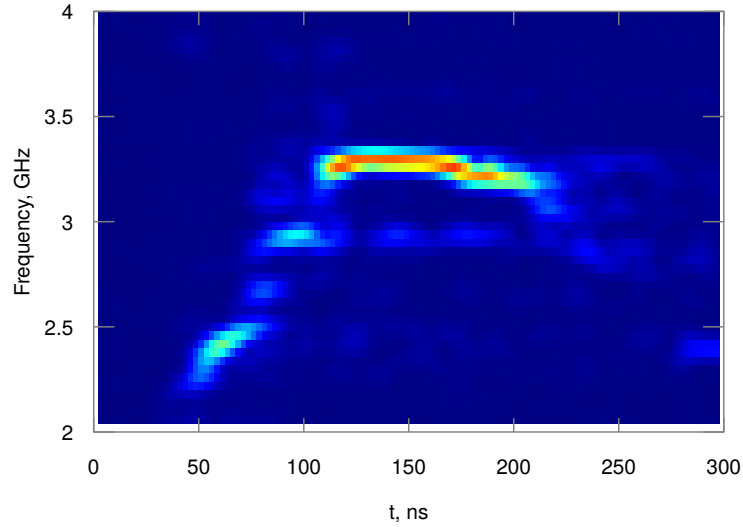


Figure 13: Spectrogram of the detected microwave signal at the most stable operation regime



Figure 14: Multicapillary cathode

Variation of the cathode-anode gap value over the range 20–16 mm demonstrated change of the main radiation frequency within the range 3.0–4.16 GHz (see Fig. 15). In each diagram zone, which corresponds to the fixed cathode-anode gap value, the sum of frequency spectra obtained in several experiments under similar conditions is presented. In all the experiments the frequency of radiation was mainly determined by the cathode-anode gap  $d$ , rather than beam current. Frequency was proportional to  $\sim 1/d$  with small variations due to current change, for example: for cathode-anode gap 16 mm change of the beam current from 15 to 18.5 kA (i.e.  $16.8 \text{ kA} \pm 10\%$ ) resulted in frequency variations within  $\pm 2\%$  range (see Fig. 15).

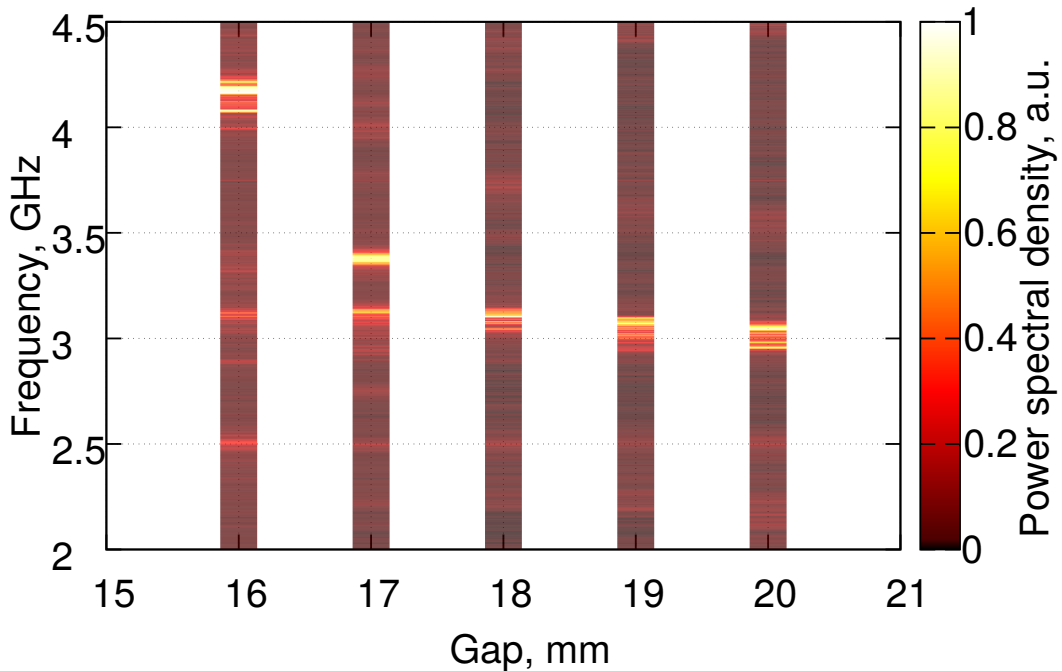


Figure 15: Comparison of reflex triode spectra obtained for different cathode-anode gap values.

Thus, HPM pulses produced by the reflex triode with the multicapillary cathode had stable frequency and power about 200 MW. Duration of current pulse determined that of radiation pulse: increase of current FWHM from 150 to 250 ns caused growth of microwave pulse duration from 50 to 150 ns.

## 5 Conclusion

We compared three types of compact HPM sources capable to produce high output power, long pulse duration and good operating stability operating without a magnetic field (see Table 2).

Parameter	Axial vircator	SCO	Reflex triode
Current pulse FWHM [ns]	150–200	200	150–250
Radiation power [MW]	300	30	200 (max. 460)
Duration of microwave pulse [ns]	50	5–10	50–150
Operation stability	low	high	high

Table 2: Comparison of different HPM sources.

For split-cavity oscillator we observed high stability, but low radiated power and pulse duration. Frequency was determined by fundamental mode in SCO cavity. Pulse duration was limited by breakdowns inside the cavity to be as low as 10 ns.

For axial vircator experiments demonstrated low reproducibility with infrequent shots with high power and efficiency: the radiated power about 300 MW was observed in several “best” shots, which were less than 10% in the total amount of all tests carried in the equivalent conditions. Radiation spectra was determined by cathode-anode gap: when the cathode-anode gap was reduced to appear below a certain value, the basic vircator frequency grew. Experimentally observed spectra fitted well the simulation results [24].

Duration of radiation pulse for shots with high output power attained 50 ns. Direct correlation of radiation pulse duration with that for current pulse was not observed.

Thus, HPM pulses produced by the reflex triode with the multicapillary cathode had stable frequency and power about 200 MW. As much as 460 MW was produced at 4.16 GHz single-frequency operation at maximum diode voltage 460 kV and amplitude of electron beam current 18 kA. Duration of current pulse determined that of radiation pulse: increase of current FWHM from 150 to 250 ns caused growth of microwave pulse duration from 50 to 150 ns. Radiation frequency was proportional to  $\sim 1/d$  with small variations due to current change, namely:  $\pm 10\%$  change in current resulted in frequency variations within  $\pm 2\%$  range.

According to the above analysis reflex triode bears the palm. Nevertheless, two other competitors still have good opportunities in case of proper considering their weak points.

## References

- [1] B.M. Marder, "The split-cavity oscillator: a high-power e- beam modulator and microwave source," IEEE Trans. Plasma Sci., vol. 20 (1992) no.3, pp. 312–331.
- [2] R. B. Miller, An Introduction to the Physics of Intense Charged Particle Beams. New York, NY, USA: Springer-Verlag, 1982.
- [3] V. L. Granatstein and I. Alexeff, Eds., High-Power Microwave Sources. Boston, MA, USA: Artech House, 1987.
- [4] J. Benford, J. A. Swegle, and E. Schamiloglu, High Power Microwaves, 2nd ed. Boca Raton, FL, USA: CRC Press, 2007.
- [5] A. N. Didenko et al., "Generation of high power rf pulses in the magnetron and reflex triode systems," in Proc. 3rd Int. Topical Conf. High-Power Electron Ion Beam Res. Technol., vol. 2. Novosibirsk, Russia (1979) pp. 683–691.
- [6] D. J. Sullivan, "High power microwave generation from a virtual cathode oscillator (viricator)," IEEE Trans. Nucl. Sci., vol. 30 (1983) no.4, pp. 3426–3428.
- [7] Raymond W. Lemke, M. Collins Clark, Barry M. Marder, "Theoretical and experimental investigation of a method for increasing the output power of a microwave tube based on the split-cavity oscillator", Journal of Applied Physics. V75, (1994), no.10, pp. 5423–5432.
- [8] Fan Zhikai, Liu Qingxiang, Chen Daibing, Tan Jie, Zhou Haijing. "Theoretical and experimental researches on C-band three-cavity transit-time effect oscillator", Science in China Ser. G Physics, Mechanics and Astronomy. V47 (2004) no.3. pp. 310-329.
- [9] He Jun-Tao, Zhong Hui-Huang, Qian Bao-Liang, Liu Yong-Gui. A new method for increasing output power of a three-cavity transit time oscillator. / Chinese Physics Letters. 2004. V21. №7. P. 1302–1305.
- [10] Relativistic Split-Cavity Oscillator/ V.G. Baryshevsky. – Research Institute for Nuclear Problems, 2014. – Mode of access: [arxiv.org/abs/1402.3403](https://arxiv.org/abs/1402.3403) Date of access: 05.01.2016.

- [11] I. Moroz, A. Rouba, Theoretical and experimental research of split-cavity oscillator, Theoretical and experimental research of split-cavity oscillator : thesis of 61st International Conference for Students of Physics and Natural Sciences «Open Readings 2018» , Vilnius, March 20-23, 2018, p. 111.
- [12] S. Anishchenko, I. Moroz, A. Rouba, Radiation instability in relativistic split-cavity oscillator, Radiation instability in relativistic split-cavity oscillator: thesis of 63st International Conference for Students of Physics and Natural Sciences “Open Readings 2020” , Vilnius, March 17-20, 2020, p. 398.
- [13] I. L. Bogdankevich et al. Influence of the Electrons Reflected from the Collector on the Parameters of a High-Current Relativistic Electron Beam. Plasma Physics Reports, Vol. 30, No. 5, 2004, pp. 376–382.
- [14] Calico S.E. et al. Experimental and theoretical investigations of a magnetically insulated line oscillator, SPIE Vol. 2557. P. 50
- [15] Haworth M.D. et al. Significant pulse-lengthening in a multigigawatt magnetically insulated transmission line oscillator, IEEE Trans. Plasma Sci. 1998. Vol. 26. No. 3. P. 312
- [16] W. Jiang, N. Shimada, S. D. Prasad, and K. Yatsui, "Experimental and simulation studies of new configuration of virtual cathode oscillator," IEEE Trans. Plasma Sci., vol. 32, no. 1, pp. 54–59, Feb. 2004.
- [17] S. A. Kitsanov et al., "S-band vircator with electron beam premodulation based on compact pulse driver with inductive energy storage," IEEE Trans. Plasma Sci., vol. 30, no. 3, pp. 1179–1185, Jun. 2002.
- [18] A. N. Didenko et al., "Reflex triode with resonant cavity as a load for inductive storage," in Proc. 11th Int. Conf. High-Power Particle Beams, vol. 1. Jun. 1996, pp. 445–448.
- [19] S. Champeaux, P. Gouard, R. Cousin, and J. Larour, "Numerical evaluation of the role of reflectors to maximize the power efficiency of an axial vircator," in Proc. 14th Int. Vac. Electron. Conf. (IVEC), May 2013, pp. 1–2.
- [20] L. Zhenxiang, S. Ting, Z. Jiande, and Q. Baoliang, "Particle simulation of an improved axially extracted vircator," Plasma Sci. Technol., vol. 5, no. 5, pp. 2007–2010, 2003.
- [21] S. Ting, W. Yong, Q. Bao-Liang, and T. Qi-Mei, "A compact vircator with feedback annulus operated in quasi-single TM 01 mode within the C band," Chin. Phys. Lett., vol. 19, no. 11, pp. 1646–1649, 2002.
- [22] L. Zhi-Qiang et al., "Simulation and experimental research of a novel vircator," Chin. Phys. Lett., vol. 25, no. 7, pp. 2566–2569, 2008.
- [23] V. Baryshevsky, A. Gurinovich, E. Gurnevich, P. Molchanov, “Experimental study of an axial vircator with resonant cavity,” IEEE Trans. Plasma Sci., vol. 43, no. 10, pp. 3507–3511, 2015.
- [24] P. V. Molchanov, E. A. Gurnevich, V. V. Tikhomirov, and S. E. Siahlo. (2014). "Simulation of an axial vircator with a three-cavity resonator." [Online]. Available: <http://arxiv.org/abs/1408.1824>



- [25] E. Gurnevich, P. Molchanov, "The effect of the electron-beam parameter spread on microwave generation in a three-cavity axial vircator," *IEEE Trans. Plasma Sci.*, vol. 43, no. 4, pp. 1014–1017, 2015.
- [26] S. Anishchenko, V. Baryshevsky, N. Belous, A. Gurinovich, E. Gurnevich, P. Molchanov, "Cumulation of high-current electron beams: theory and experiment," vol. 45, no. 10, pp. 2739–2743, 2016.
- [27] S.V. Anishchenko, V.G. Baryshevsky, A.A. Gurinovich, "Electrostatic cumulation of high-current electron beams for terahertz sources," vol. 22, 043403, 2019.
- [28] S. V. Anishchenko and A. A. Gurinovich, "Modeling of high-current devices with explosive electron emission," *Comput. Sci. Discovery*, vol. 7, no. 1, p. 015007, 2014.
- [29] S. V. Anishchenko and A. A. Gurinovich, "Modeling of explosive electron emission and electron beam dynamics in high-current devices," *J. Phys., Conf. Ser.*, vol. 490, no. 1, p. 012116, 2014.
- [30] J. J. Mankowski, X. Chen, J. C. Dickens, and M. Kristiansen, "Experimental optimization of a reflex triode virtual cathode oscillator," in *Proc. Int. Conf. High-Power Particle Beams (BEAMS)*, Jul. 2004, pp. 426–429.
- [31] L. Liu, L. M. Li, X. P. Zhang, J. C. Wen, H. Wan, and Y. Z. Zhang, "Efficiency enhancement of reflex triode virtual cathode oscillator using the carbon fiber cathode," *IEEE Trans. Plasma Sci.*, vol. 35, no. 2, pp. 361–368, Apr. 2007.
- [32] V. P. Grigoryev, A. G. Zherlitsyn, T. V. Koval, G. V. Melnikov, and P. Ya Isakov, "Mode structure research of a field in the triode with the virtual cathode with an active feedback," in *Proc. 14th Symp. High Current Electron.*, Tomsk, Russia, 2006, vol. 40, no. 11, pp. 372–375.
- [33] Y. Chen, J. Mankowski, J. Walter, M. Kristiansen, and R. Gale, "Cathode and anode optimization in a virtual cathode oscillator," *IEEE Trans. Dielectr. Electr. Insul.*, vol. 14, no. 4, pp. 1037–1044, Aug. 2007.
- [34] A.G. Zherlitsyn, G.V. Mel'nikov, P.Ya. Isakov, "Effect of feedback on the microwave radiation in a triode with a virtual cathode," *J. Commun. Technol. and Electron.*, vol. 52, no. 7, pp. 798–802, 2007.
- [35] J. Benford, D. Price, H. Sze, and D. Bromley, "Interaction of a vircator microwave generator with an enclosing resonant cavity," *J. Appl. Phys.*, vol. 61, no. 5, pp. 2098–2100, 1987.
- [36] G. Z. Liu et al., "Coaxial cavity vircator with enhanced efficiency," *J. Plasma Phys.*, vol. 74, no. 2, pp. 233–244, 2008.
- [37] W. Yang, Z. Dong, and Y. Dong, "Numerical studies of a new-type vircator with a resonant cavity," *IEEE Trans. Plasma Sci.*, vol. 38, no. 9, pp. 2428–2433, Sep. 2010.
- [38] V. Baryshevsky, A. Gurinovich, E. Gurnevich, and P. Molchanov, "Experimental study of a triode reflex geometry vircator," *IEEE Trans. Plasma Sci.*, vol. 45, pp. 631–635, 2017.

- [39] T. Queller, J. Gleizer, and Y. Krasik, “High-current long-duration uniform electron beam generation in a diode with multicapillary carbon-epoxy cathode,” *J. Appl. Phys.*, vol. **114**, 123303, 2013.